Journal of Materials Chemistry B

Photoinduced reconfiguration to control the protein-binding affinity of azobenzene-cyclized peptides

Journal:	*Journal of Materials Chemistry B*
Manuscript ID	TB-ART-05-2020-001189.R1
Article Type:	Paper
Date Submitted by the Author:	30-May-2020
Complete List of Authors:	Day, Kevin; North Carolina State University, Chemical & Biomolecular Engineering Schneible, John; North Carolina State University, Chemical and Biomolecular Engineering Young, Ashlyn; UNC/NCSU Joint Department of Biomedical Engineering, Biomedical Engineering Pozdin, Vladimir; North Carolina State University, Department of Electrical and Computer Engineering Gaffney, Lewis; North Carolina State University College of Engineering, Biomedical Engineering Prodromou, Raphael; North Carolina State University, Chemical & Biomolecular Engineering Freytes, Donald; North Carolina State University College of Engineering, Biomedical Engineering Daniele, Michael; North Carolina State University, Department of Electrical and Computer Engineering; North Carolina State University and University of North Carolina, Chapel Hill, Joint Department of Biomedical Engineering Menegatti, Stefano; North Carolina State University, Chemical & Biomolecular Engineering

ARTICLE

Received 00th January 20xx,
Accepted 00th January 20xx
DOI: 10.1039/x0xx00000x

Photoinduced reconfiguration to control the protein-binding affinity of azobenzene-cyclized peptides†

Kevin Day,[a,§] John D. Schneible,[a,§] Ashlyn T. Young,[b,§] Vladimir A. Pozdin,[b,c,d] Lewis A. Gaffney,[b] Raphael Prodromou,[a] Donald O. Freytes,[b] Michael Daniele,[b,e,*] and Stefano Menegatti[a,f,*]

The impact of next-generation biorecognition elements (ligands) will be determined by the ability to remotely control their binding activity for a target biomolecule in complex environments. Compared to conventional mechanisms for regulating binding affinity (pH, ionic strength, or chaotropic agents), light provides higher accuracy and rapidity, and is particularly suited for labile targets. In this study, we demonstrate a general method to develop azobenzene-cyclized peptide ligands with light-controlled affinity for target proteins. Light triggers a *cis/trans* isomerization of the azobenzene, which results in a major structural rearrangement of the cyclic peptide from a non-binding to a binding configuration. Critical to this goal are the abiliy to achieve efficient photo-isomerization under low light dosage and the temporal stability of both *cis* and *trans* isomers. We demonstrated our method by designing photo-switchable peptides targeting vascular cell adhesion marker 1 (VCAM1), a cell marker implicated in stem cell function. Starting from a known VCAM1-binding linear peptide, an ensemble of azobenzene-cyclized variants with selective light-controlled binding were identified by combining *in silico* design with experimental characterization via spectroscopy and surface plasmon resonance. Variant cyclo$_{AZOB}$[G-VHAKQHRN-K] featured rapid, light-controlled binding of VCAM1 ($K_{D,Trans}/K_{D,Cis}$ ~ 130). Biotin-cyclo$_{AZOB}$[G-VHAKQHRN-K] was utilized to label brain microvascular endothelial cells (BMECs), showing co-localization with anti-VCAM1 antibodies in *cis* configuration and negligible binding in *trans* configuration.

Introduction

Inducible affinity interactions between ligand and target biomolecules are the underlying functions governing biological systems. The ability to design synthetic ligands whose biorecognition can be activated and controlled using remote and biocompatible stimuli is key to engineer next-generation biomimetic systems. Mainstream engineered ligands, like antibodies and aptamers,[1–4] enable sensitive detection and sorting of biological targets (*e.g.*, proteins, viruses, and cells) in complex media.[5,6] Their biorecognition activity, while strong and selective, is innate and cannot be activated on demand. Adjusting the composition, concentration, and pH of the aqueous environment provides some control over binding strength, but often at the expense of the bioactivity and viability of the target. The ability to design synthetic ligands whose affinity for a target can be activated rapidly and remotely, using external stimuli that do not adversely impact the integrity of the target, is a much sought-after goal in modern ligand engineering.

Peptides represent ideal scaffolds for developing dynamically regulated ligands, owing to their excellent biorecognition activity, modular assembly, and affordable manufacturing at large scale with no batch-to-batch variability.[7] In particular, peptides with constrained conformation (*e.g.*, cyclic peptides) feature superior target affinity and selectivity – in some instances, on par with antibodies – as well as high biochemical stability.[8–10] Furthermore, cyclic peptides can be engineered to integrate stimuli-responsive moieties that provide remote control over target-binding affinity independently of the physicochemical conditions of the environment. Of particular interest in this regard are photochromic switches, such as azobenzenes, hemithioindigos, and spiropyrans/spirooxazines, which respond to specific light wavelengths and intensities by rearranging their structure. When utilized as peptide cyclization linkers, photochromic switches can reconfigure the peptide structure upon photo-isomerization.[11–18] This mechanism can be harnessed to remotely activate the selective binding of the peptide for a target biomolecule, resulting in adsorption on a substrate or labelling in solution.

In this study, we sought to develop a novel family of azobenzene-cyclized peptide affinity ligands that are selective, sterically inconspicuous, rapidly activated, and thermally stable (*note:* we adopted

[a] *Department of Chemical and Biomolecular Engineering, North Carolina State University, 911 Partners Way, Raleigh, North Carolina, United States.*
[b] *Joint Department of Biomedical Engineering, North Carolina State University – University of North Carolina Chapel Hill, North Carolina, United States.*
[c] *Department of Electrical and Computer Engineering, Florida International University, 10555 W. Flagler St., Miami, Florida, United States*
[d] *Department of Mechanical and Materials Engineering, Florida International University, 10555 W. Flagler St., Miami, Florida, United States*
[e] *Department of Electrical and Computer Engineering, North Carolina State University, 890 Oval Drive, Raleigh, North Carolina, United States.*
[f] *Biomanufacturing Training and Education Center, North Carolina State University, 850 Oval Dr, Raleigh, North Carolina, United States*
** Corresponding authors; emails: smenega@ncsu.edu, mdaniel6@ncsu.edu*
§ Denotes Equal Contribution

† Electronic Supplementary Information (ESI) available: "Druggability" analysis of VCAM1, extended photophysical characterization, circular dichroism spectra, ellipsometry results for SPR chips, and qRT-PCR results for VCAM1 expression. See DOI: 10.1039/x0xx00000x

azobenzene as photochromic switch owing to its ease of synthesis and commercial availability to ensure the translational potential of this technology). To this end, we have developed a method for converting known linear protein-binding peptides into an azobenzene-cyclized framework (Fig. 1). This comprises a protein-binding peptide segment, the azobenzene cyclization linker, connecting spacers, and a reporter (*e.g.*, a fluorescent dye or biotin). The proposed cyclization geometry provides an optimal balance between structural flexibility and rigidity, which enables rapid and high-yield photo-isomerization under moderate light intensity, and ensures temporal and thermal stability of both *trans* and *cis* isomers.

To demonstrate our method, we chose the Vascular Cell Adhesion Marker 1 (VCAM1) as protein target, and the linear VCAM1-binding peptide VHPKQHR as reference sequence.[19] VCAM1 is a cell surface sialoglycoprotein implicated in directing downstream lineages of human hematopoietic progenitor cells (HPCs).[20] VCAM1 negative ($VCAM1^-$) HPCs give rise to lymphoid progenitors, while $VCAM1^+$ HPCs result in myeloid progenitors, suggesting that VCAM1 expression in HPCs represents a branching point between the lymphoid and myeloid lineages.[21,22] Sorting lineage-committed HPCs into lymphoid ($VCAM1^{-/low}$) and myeloid ($VCAM1^+$) has the potential to enable stem cell therapies for treating leukemia, lymphoma, cardiac failure, neural disorders, autoimmune diseases, metabolic or genetic disorders. The VCAM1-binding linear peptide has been identified via phage-display screening in apolipoprotein E-deficient mice and has been utilized as a ligand for VCAM1 in numerous applications.[23–26]

The design method begins with the *in silico* analysis of the crystal structure of VCAM1 (PDB IDs: 1VCA) using a "druggability" test to identify binding sites for peptide binding.[27,28] The information on size, structure, and physicochemical properties of the putative binding sites was used to design a set of 25 peptide variants in the form $cyclo_{AZOB}$[G-VH(X)KQHR(Z)-K]-GSG (Fig. 1) where (X) and (Z) are interchangeably A, D, N, P, or S. The structures of the azobenzene-cyclized peptides were generated by molecular dynamics (MD)[29,30] and docked *in silico*[31,32] on VCAM1 to identify leads with conformation-dependent binding. Selected complexes were then refined by MD simulations to select azobenzene-cyclized variants with predicted high binding strength (*i.e.*, either $\Delta G_{B,Trans}$ or $\Delta G_{B,Cis}$ < - 8 kcal·mol^{-1}) and loss of binding upon photo-isomerization (*i.e.*, $|\Delta\Delta G_B| = |\Delta G_{B,Trans} - \Delta G_{B,Cis}| > 2.5$ kcal·mol^{-1}).[33,34]

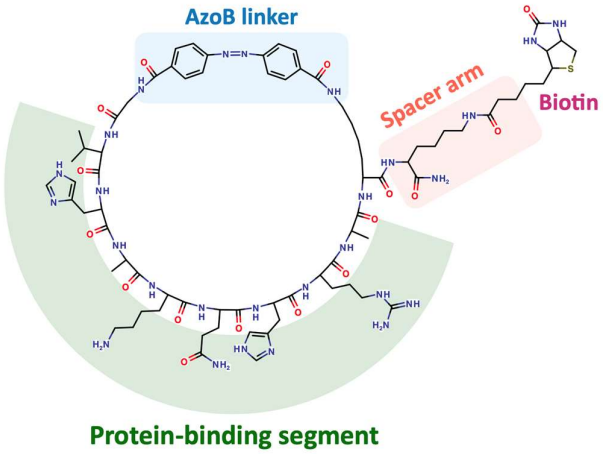

Fig. 1 Structure of the proposed azobenzene-cyclized peptides.

Three azobenzene-cyclized peptides selected from *in silico* screening were characterized to evaluate their *(i)* VCAM1 binding activity by surface plasmon resonance (SPR), *(ii)* kinetics of photo-isomerization upon exposure to light by UV/Vis spectroscopy, and *(iii)* thermal stability of the *cis* isomers. Variant $cyclo_{AZOB}$[G-VHAKQHRN-K] in particular showed efficient photo-isomerization and an ample affinity shift ($K_{D,Trans}/K_{D,Cis}$ ~ 130), which ensured efficient light-controlled binding of VCAM1. Finally, the peptide was fused with biotin and utilized as a light-activated label for brain microvascular endothelial cells (BMECs); VCAM1 expression was induced by a synergistic treatment of Interleukin-4 (IL-4) with lipopolysaccharide (LPS) and confirmed by immunohistochemical staining and RT-qPCR. Cell imaging by fluorescence microscopy confirmed binding of VCAM1 on BMECs by the *cis* isomer of $cyclo_{AZOB}$[G-VHAKQHRN-K], which afforded fluorescent labelling of cells with intensity proportional to the cell surface density of VCAM1, while showing negligible binding in *trans*. These results demonstrate the effectiveness of our design and selection methods for developing peptide ligands whose target-binding affinity can be rapidly activated via light-controlled structural reconfiguration.

Experimental

Materials

N,N'-Dimethylformamide (DMF), dichloromethane (DCM), ethanol, HPLC-grade acetonitrile, HPLC-grade water, and endogenous biotin blocking kit were from ThermoFisher Scientific (Waltham, MA). Protected amino acids, piperidine, trifluoroacetic acid (TFA), diisopropylethylamine (DIPEA), Rink amide resin (100-200 mesh, functional density ~ 0.6 mmol g^{-1}), and Hexafluorophosphate Azabenzotriazole Tetramethyl Uronium (HATU) were purchased from ChemImpex Inc. (Wood Dale, IL). Purified $cyclo_{AZOB}$[G-VHAKQHRN-K]-K(Biotin) was sourced from the peptide synthesis facility at UNC Chapel Hill. Bovine serum albumin, Alexa Fluor 488-labeled streptavidin (AF488-streptavidin), DAPI nuclear stain, anti-human VCAM1 (CD106) rabbit monoclonal antibody and polyclonal goat anti-rabbit antibody, azobenzene-4,4'-dicarbonyl dichloride, glycine, glacial acetic acid, diethyl ether, triethylamine (TEA), triisopropylsilane (TIPS), ethanedithiol (EDT), Tween 20, 1M aqueous NaOH, phosphate-buffered saline (PBS) pH 7.4, acetic anhydride, Kaiser test kit, and were from Millipore Sigma (St. Louis, MO). Azido-PEG-thiol (N_3-PEG-SH, MW = 600 Da) was from Nanocs Inc. (New York, NY), while amine-PEG-thiol (NH_2-PEG-SH, MW = 2,000 Da) and hydroxyl PEG thiol (OH-PEG-SH, MW = 1,000 Da) were from Creative PEGWorks (Chapel Hill, NC). Glass sensor chips (12 x 20 x 0.5 mm) sputtered with a 50 nm gold layer were from KSV Instruments OY (Helsinki, Finland). Nitrogen gas was obtained from Airgas National Welders (Raleigh, NC). VCAM1 was obtained from SinoBiologicals (Beijing, China). Brain microvascular endothelial cells (BMECs) were obtained from ATCC (Manassas, VA).

Peptide synthesis and characterization

Synthesis

The linear peptide precursors VHGKQHRP-K*, G-VHAKQHRN-K*-Prg, G-VHAKQHRP-K*-Prg, G-VHNKQHRP-K*-Prg, G-VHPKQHRS-K*-Prg,

G-VHNKQHRS-K*-Prg, G-VHPKQHRP-K*-Prg, and VHPKQHR-GSG-Prg (Prg: propargyl-glycine) were synthesized on Rink amide polystyrene resins via Fmoc/tBu chemistry using standard protecting groups for all amino acids except K* (Fmoc-Lys(Mtt)-OH).[35–37] All amino acid conjugations were conducted using a Biotage Alstra Initiator (Biotage, Uppsala, Sweden) by performing 3 coupling steps with protected amino acid (5 equivalents), HATU (5 eq.), and DIPEA (10 eq.) at 75°C for 5 min in DMF. Fmoc removal occurred in 20% piperidine in DMF at RT for 20 min. Upon completion of chain elongation, the Fmoc group on the N-terminus was removed, and the resin was copiously rinsed with DCM and vacuum dried. The dry resin was swollen in DCM (dried over molecular sieves), cooled to 0°C, and anhydrous TEA (1.2 eq.) and azobenzene-4,4'-dicarbonyl dichloride (1.2 eq. in anhydrous DCM) were added dropwise at 0°C over 10 min. The system was equilibrated at RT and the reaction was allowed to proceed overnight. The resin was copiously rinsed with DCM and the azobenzene conjugation was confirmed by Kaiser's test.[38] The Mtt protecting group on K* was removed by incubating the resin with 2/5/93 (TFA/TIPS/DCM) for 5 min. Completion of K* deprotection was verified by Kaiser's test. After rinsing with DCM and DMF, the peptide was cyclized through reaction of the carboxyl group on the azobenzene linker with the ε-amino group of K*, by incubating the resin with HATU (5 eq.) and DIPEA (10 eq.) in DMF for 10 min at 75°C. Completion of the cyclization reaction was verified by Kaiser's test. The resin was finally rinsed with DMF, DCM, and dried under nitrogen then incubated for 2 hrs at RT 10 mL g^{-1} of 95/2.5/2.5 (TFA/TIPS/water). The peptide was precipitated by drop-wise addition into ice-cold diethyl ether. The precipitate was copiously rinsed with diethyl ether, dissolved in 50/50 (acetonitrile/water), and lyophilized. The crude peptide powder was purified by preparative C18 HPLC and lyophilized.

Peptide photo-isomerization

All spectroscopy measurements were performed using Cary 60 spectrometer equipped with a custom cuvette holder on a Peltier stage to maintain the peptide solutions at 37°C. Orthogonal to the spectrometer beam, the peptide solution was irradiated with a BlueWave 200 lamp (Dymax, Torrington, CT) to induce photoisomerization. A volume of 700 µL of $cyclo_{AZOB}$[VHGKQHRP-K*] in MilliQ water at either at 0.15 mM, 0.38 mM, or 1.5 mM was initially placed in quartz micro cuvette (Thorlabs, Newton, NJ). The cuvette was placed in the spectrometer with a 10 mm pathlength for UV-Vis spectroscopy and a 2 mm pathlength for irradiance. A UV bandpass filter (BP305-390, Thorlabs, Newton, NJ) was used to achieve *trans*-to-*cis* isomerization, whereas a 420 nm longpass (LP420, Edmund Optics, Barrington, NJ) filter was used for *cis*-to-*trans* isomerization. Spectra of the lamp and filtered outputs are reported in the ESI. The incident irradiance power was calculated by measuring the output power using an AccuCal 50 radiometer (Dymax, Torrington, CT). The kinetics of photo-isomerization was measured by monitoring the absorption at 350 nm. The absorbance *vs.* time data was fitted against an exponential function to derive the kinetic constant of photo-isomerization κ (s^{-1}). The values of κ were obtained for light intensities between 10 and 50 $mW{\cdot}cm^{-2}$. The rate of thermal reverse isomerization (*cis*-to-*trans*) was evaluated by monitoring the absorbance at 350 nm of a 0.15 mM solution of $cyclo_{AZOB}$[VHGKQHRP-K*], initially conditioned in *cis* configuration and allowed to relax in the dark over 60 hrs with absorption measurements taken every 15 min.

Circular Dichroism (CD)

A solution of $cyclo_{AZOB}$[VHGKQHRP-K*] at 200 µM in PBS was placed in two 1 mL quartz micro fluorescence cuvettes (Thorlabs, Newton, NJ). The peptides in solution were conditioned to either *cis* or *trans* configuration as described in the previous section, and further diluted with PBS to reach a final concentration of 80 µM. The CD spectra of the solutions of *cis* and *trans* peptide isomer were measured on a J-715 spectropolarimeter (JASCO, Oklahoma City, OK) through the 10 mm path length of the quartz cell. The samples were scanned from 190 to 260 nm, at a resolution of 1.0 nm and a scanning speed of 100 nm min^{-1}. For each sample, five scans were averaged together and a 5-point moving average was applied.

Binding affinity using surface plasmon resonance (SPR)

Surface plasmon resonance SPR sensor chips were prepared, characterized, and utilized for affinity measures as described by Islam *et al.*[39,40] The sensor chips were initially coated with a PEG-based self-assembled monolayer (SAM), on which the test azobenzene-cyclized peptides and the linear precursor VHPKQHR were conjugated to the surface via azide-alkyne "click chemistry";[41] sensor chips coated with hydroxyl-PEG-thiol only were utilized as negative controls. Three gold sensors per ligand were prepared and analyzed by variable angle spectroscopic ellipsometry (VASE, J.A. Woollam Co.) to measure ligand density. The measurements of peptide-VCAM1 dissociation constant (K_D) were performed at the UNC Macromolecular Interactions Facility.[39,40] Briefly, sensor chips functionalized with azobenzene-cyclized peptides were initially conditioned to their *cis* or *trans* isomers and contacted with a solution of human VCAM1 at concentrations ranging between 0.01 and 1 mg mL^{-1} in PBS.

***In silico* design of VCAM1-binding peptides**

The crystal structures of the extracellular domain of VCAM1 (PDB: 1VCA)[42] were subjected to standard protein preparation using Schrödinger's ProteinPrep Wizard to search for and correct missing atoms and/or entire side chains (using PRIME software), remove extra salts and non-binding ligands, add explicit hydrogens, assign tautomeric states with EPIK, optimize hydrogen-bonding networks, and minimize the protein's energy with the OPLS3e force field.[43–45] The adjusted structure was then subjected to a "druggability" study using SiteMap to identify putative binding sites capable of accommodating azobenzene-cyclized peptides.[46,47] To this end, the SiteMap (Schrödinger, New York, NY) algorithm identifies binding pockets by placing spherical 'site points' across the protein surface. These site points are then clustered together based on *(i)* their ability to form favorable protein-ligand or protein-protein interactions, *(ii)* solvent exposure, and *(iii)* hydrophobic/philic character. Finally, regions that possess a sufficient number of site points and volume are globally scored using an S-score and D-score. The S-score represents the likelihood of the protein's surface to be a binding pocket, while the D-score provides a measure of the pocket's 'druggability.' S-score and D-score values greater than or equal to 0.7 and 0.9 respectively were considered favorable pockets for ligand binding. Herein, the SiteMap analysis was performed with the default settings and the 'detect shallow binding sites' option selected, which adjusts amino acid atomic van der Waals radii to be more accommodating for peptide binding when locating potential binding pockets.

An ensemble of 25 peptide variants of VHPKQHR in the azobenzene-cyclized form $cyclo_{AZOB}$[G-VH(X)KQHR(Z)-K]-GSG were designed by varying the positions (X) and (Z) using amino acids A, D, N, P, S, or R. The structures of the linear precursor VHPKQHR and the azobenzene-cyclized variants as both *cis* and *trans* isomers were initially designed using the molecular editor Avogadro, and equilibrated by molecular dynamics in the GROMACS simulation package[29,30,48] using the OPLS all-atom force field[49,50] and periodic boundary conditions.[51–53] The force-field parameters for the azobenzene linker were derived from density functional theory using GAUSSIAN98.[51] Every peptide was individually placed in a simulation box with periodic boundary conditions containing 800 water molecules (TIP3P water model). The solvated system was initially minimized by running 10,000 steps of steepest gradient descent, heated to 300 K in an NVT ensemble for 250 ps with 1 fs time steps, and equilibrated to 1 atm by running a 500-ps NPT simulation with 2 fs time steps. The production run for every peptide was performed in the NPT ensemble, at constant T = 300 K using the Nosé-Hoover thermostat[54–56] and constant P = 1 atm using the Parrinello-Rahman barostat.[57,58] The atomic coordinates were saved every 2 ps. The leap-frog algorithm was used to integrate the equations of motion, with integration steps of 2 fs, and all of the covalent bonds were constrained by means of the LINCS algorithm.[59] The short-range electrostatic and Lennard-Jones interactions were calculated within a cutoff of 1.0 nm and 1.4 nm, respectively, whereas the particle-mesh Ewald method was utilized to treat the long-range electrostatic interactions.[60,61] The non-bonded interaction pair-list was updated every 5 fs, using a cutoff of 1.4 nm.

The peptides were then docked *in silico* against the putative binding sites on VCAM1 using the docking software HADDOCK (High Ambiguity Driven Protein-Protein Docking, v.2.1).[31,32] Default HADDOCK parameters (*e.g.*, temperatures for heating/cooling steps, and number of molecular dynamics sets per stage) were used. All the residues on each binding site (solvent accessibility of 50% or greater) were defined as "active", whereas the residues surrounding the binding sites were defined as "passive". All variable amino acid positions on the peptide ligands were also denoted as "active", while the GSG tripeptide spacer was defined as not being involved in the interaction to account for the directionality of binding. Docking proceeded through a 3-stage protocol: *(i)* rigid, *(ii)* semi-flexible, and *(iii)* water-refined fully flexible docking. A total of 1000, 200, and 200 structures were calculated at each stage, respectively. Final structures were grouped using a minimum cluster-size of 20 (10% of the total water refined calculated structures) with a Cα RMSD < 7.5 Å using ProFit (http://www.bioinf.org.uk/software/profit/). Once the clusters were identified for each peptide-VCAM1 complex pair, FireDock and XScore were used to score the complexes;[33,34] FireDock is an efficient method re-scoring of protein-protein docking solutions, while Xscore computes the dissociation of a protein-ligand complex using an empirical equation that considers energetic factors in a protein-ligand binding process. The selected binding poses of the peptide variants, in both their *cis* and *trans* forms, on the putative binding sites of VCAM1 were then refined via 100-ns atomistic molecular dynamics (MD) simulations using the GROMACS simulation package. The peptide-VCAM1 complexes were embedded in a cubic periodic box of 9.7 nm side lengths and solvated with 30,000 TIP3P water molecules. The MD simulations were performed at 300 K and 1 atm using the Amber99SB force field. The MM/GBSA method was used for post-processing of the peptide-VCAM1 complexes derived from MD simulations to estimate the free energy of binding (ΔG_B).[62,63] if complexes had conflicting docking score or MM-GB/SA ranks, then the complex was discarded. If the two rankings agreed, then the complex was saved. The variants that possessed strong binding in either *cis* or *trans* configuration (*i.e.*, $\Delta G_{B,Trans}$ or $\Delta G_{B,Cis} < -8$ kcal mol^{-1}) and loss of binding upon photo-isomerization (*i.e.*, $|\Delta\Delta G_B| = |\Delta G_{B,Trans} - \Delta G_{B,Cis}| > 2.5$ kcal mol^{-1}) were selected for experimental analysis.

***In vitro* evaluation of VCAM1-binding peptides**

Cell culture and VCAM1 expression

Human brain microvascular endothelial cells (BMEC) (cAP-0002; Angioproteomie, Boston, MA, US) were cultured using Microvascular Endothelial Cell Growth Medium 2 (EGM-2 MV) (CC-3202; Lonza, Basel, Switzerland). Human dermal fibroblasts (HDFn) (PCS-201-010; ATCC, Manassas, VA, US) were cultured using Dulbecco's modified eagle's medium (DMEM) (10013CV; Corning, Corning, NY, US) supplemented with 10% fetal bovine serum (FBS) (25-514H; Genesee Scientific, Cajon, CA, US) and 1X penicillin- streptomycin (30-002-CI; Corning, Corning, NY, US). Human umbilical vein endothelial cells (HUVEC) (C2519A; Lonza, Basel, Switzerland) were cultured using Endothelial Cell Growth Medium 2 (EGM-2) (CC-3162; Lonza, Basel, Switzerland). Cells were cultured in an incubator maintaining an atmosphere of 5% CO_2 at 37°C and 100% humidity. A glass bottomed 96 well plate was pretreated with 50 µg of fibronectin (356008; Corning, Corning, NY, US) in deionized water for 1 hr. Fibronectin solution was aspirated and 1×10^4 BMECs, HDFns, or HUVECs per well were seeded in 100 µL of EGM-2 MV media, DMEM with 10% FBS, or EGM-2 media, respectively. Cells were allowed to adhere for 24 hrs. BMECs were treated with three conditions: *(i)* media only, *(ii)* 1 µg mL^{-1} lipopolysaccharide for 24 hrs, or *(iii)* 100 ng mL^{-1} IL-4 for 1 hr followed by 23 hrs of treatment with 1 µg mL^{-1} lipopolysaccharide. After treatment period, cells were fixed with 4% paraformaldehyde in 1x PBS for 10 min at RT and washed twice with 1x PBS. BMECs were permeabilized with 0.1% Triton X-100 in 1x PBS for 5 min at RT and washed twice with 1x PBS. Cells were then blocked for 1 hr with 2% w/v bovine serum albumin (BSA) at RT.

RT-qPCR quantification of VCAM1 expression

Cells were cultured and treated as described in the previous section. To quantify gene expression, cells were lysed in TRK lysis buffer, then RNA from samples were isolated using EZNA isolation kit (Omega Bio-Tek, Norcross, GA). cDNA templates were created from the RNA samples using a Go Script reverse transcriptase kit (Promega, Madison, WI). Primers target genes were determined from PrimerBank from Harvard University and selected for specificity with the NCBI Primer BLAST tool; those primers were: AAGGTGAAGGTCGGAGTCAAC (Forward – GAPDH), GGGGTCATTGATGGCAACAATA (Reverse – GAPDH), GGGAAGATGGTCGTGATCCTT (Forward – VCAM1), and TCTGGGGTGGTCTCGATTTTA (Reverse – VCAM1). cDNA samples were analyzed using SYBR Master Mix (Applied BioSystems, Foster City, CA) with a QuantStudio 3 real time PCR machine (ThermoFisher, Waltham, MA). Relative gene expression of cell-specific genes was calculated by determining the change in VCAM1 expression relative to the housekeeping gene GAPDH, following Equation 1:

$$\Delta CT = 2^{-[CT_{VCAM1} - CT_{GAPDH}]} \quad (1)$$

where CT is the threshold cycle.

Cell-labelling with cyclo$_{AZOB}$[G-VHAKQHRN-K*]

Cells were fixed and permeabilized as described above and blocked using the endogenous biotin blocking kit (ThermoFisher, Waltham, MA). First, cells were incubated with 100 µL of the streptavidin "solution A" for 30 min at RT. The cells were then washed thrice with PBS, incubated with 100 µL of biotin solution "solution B" for 30 min RT, washed again, and stored in PBS overnight at 4°C. The cells were finally stained in three conditions; *(i)* cyclo$_{AZOB}$[G-VHAKQHRN-K*]-K(Biotin) only, *(ii)* anti-VCAM1 antibody only, or *(iii)* co-localized with both peptide and antibody.

For peptide-only staining, a solution of cyclo$_{AZOB}$[G-VHAKQHRN-K*]-K(Biotin) at 0.1 mg mL^{-1} in PBS was initially split in two pools: one was conditioned into the *cis* configuration (VCAM1-binding), while the other was conditioned into the *trans* configuration (VCAM1-non-binding), as described above. After irradiation, both peptide solutions were diluted with PBS to a final concentration of 50 µg mL^{-1}. A volume of 100 µL of peptide solution was added to the fixed cells and incubated for 2 hrs at RT in dark. The fixed cells were then washed copiously with PBS, then stained with 100 µL of AF488-streptavidin (2 µg mL^{-1}) in PBS for 35 min at RT, washed with PBS, and stained with 100 µL of 300 nM DAPI in PBS for 5 min at RT.

For antibody-only staining, 100 µL solution of primary anti-VCAM1 rabbit monoclonal antibody (abcam, Cambridge, UK) at 1.75 µg mL^{-1} in PBS was incubated with the fixed cells overnight at 4°C. After incubation, the cells were washed with 1X PBS and 100 µL of AF594-labeled anti-rabbit goat polyclonal antibody (Abcam, Cambridge, UK) at 4 µg mL^{-1} was incubated with the cells for 2 hrs at RT in the dark. The wells were washed with 1X PBS, and DAPI stained.

For co-localized staining, the fixed cells were stained with cyclo$_{AZOB}$[G-VHAKQHRN-K*]-K(Biotin) and subsequently with anti-VCAM1 antibody, as described above.

Cell Imaging

Stained cells were imaged using a Zeiss LSM 710 confocal microscope (Carl Zeiss AG, Oberkochen, Germany). The resulting images were processed using ImageJ software. The fluorescence quantification was determined by averaging the raw intensity measurement of 9 images at 20x magnification for each condition. Final values of relative intensity were obtained by normalizing the averaged value to the maximum and minimum measured intensity across all conditions. Error bars are reported as standard error. Statistics were done using a 2-tailed t-test and p values < 0.05 (*) were considered statistically significant.

Results and Discussion

Azobenzene-cyclized peptide design

Azobenzene linkers have been extensively utilized to endow peptides and small proteins with the ability to reconfigure their structure reversibly upon exposure to light.[64,65] Recently, a novel set of azobenzene linkers have been developed, which feature electron-donating/-withdrawing groups in the *ortho* and *para* position to the azo group. These modifications enable photo-isomerization under biocompatible light wavelengths (*i.e.*, red, far-red, and infrared) and tuning of the thermal *cis*-to-*trans* isomeric relaxation.[66,67] While the structural and photokinetic properties of azobenzene-constrained peptides and proteins have been extensively studied, both experimentally[68,69] and computationally,[51–53] less effort has been dedicated to the engineering of azobenzene-peptide hybrids with light-controlled biorecognition activity.[70–74] Bellotto *et al.* have identified streptavidin-targeting light-responsive peptides by screening phage-display libraries;[72] the selected peptides exhibited a ~ 3-fold shift in binding strength upon light exposure, with a dissociation constant (K_D) varying between 2.2 µM (*trans* isomer) and 6.7 ± 2 µM (*cis* isomer). Using the same peptide cyclization strategy and phage-display library technique, Jafari *et al.* identified azobenzene-cyclized peptide ligands against streptavidin[75] with a ~4.5-fold shift in K_D. Using a rational design approach, Woolley *et al.* modified a leucine zipper DNA-binding protein by crosslinking two cysteine residues using an azobenzene linker;[74] when the azobenzene is in *cis* configuration, the protein maintains its α-helical structure and its DNA-binding activity; vice versa, when in *trans*, the azobenzene disrupts the structure of the protein, resulting in a 20-fold decrease in binding strength.

Following on this work, we sought to develop peptides that feature *(i)* rapid photo-isomerization kinetics, *(ii)* a large shift in protein-binding strength between *trans* and *cis* isomers, and *(iii)* high thermal stability in *cis* configuration. To this end, we have devised an azobenzene-cyclized peptide structure (Fig. 1), constructed by head-to-side-chain cyclization between the peptide N-terminal α-amine group and the ε-amine group on the C-terminal lysine using homobifunctional azobenzene-4-4'-dicarbonyl linker. The length of the protein-binding peptide segment set at 8 amino acids and cyclization through the C-terminal lysine residue were adopted to achieve a balance between chain flexibility, which increases with the number of residues and enables rapid photoisomerization, and chain rigidity, which promotes binding affinity and stability of the isomers. The observations collected in this study indicate that the proposed design indeed affords efficient photo-isomerization under moderate light dose, which translates into a remarkable shift in protein-binding affinity, and a high thermal and temporal stability of the *cis* isomer.

In silico design of VCAM1-binding peptides

The linear VCAM1-binding peptide VHPKQHR, discovered by phage-display screening,[23–25] was adopted as precursor for the design of azobenzene-cyclized light-responsive variants. This peptide has been demonstrated to target VCAM1 with high affinity and selectivity in numerous works.[25,26] Our method for designing light-responsive variants of VHPKQHR requires the identification of putative binding sites on VCAM1 that are compatible with the size and shape of 8-mer cyclic peptides, and the production of the crystal structure of the *trans* and *cis* isomers of the azobenzene-cyclized variants. To this end, the crystal structure of VCAM1 (PDB ID: 1VCA) was evaluated *in silico* by performing a "druggability" analysis of the protein surface[27,28] using Schrödinger's SiteMap software.[46,47] Five binding pockets (S1-S5 in Fig. S1) with adequate size, shape, physicochemical properties, and solvent exposure were identified as putative binding sites for the azobenzene-cyclized peptides[76,77]. They were ranked according to two scores, namely Site Score and Druggability Score;[47] the SiteMap outputs for sites S1-S5 are listed in Table S1. All sites are characterized by high pocket exposure (> 0.8) and low enclosure scores (< 0.4), and are relatively hydrophilic as determined by SiteMap's balance score.

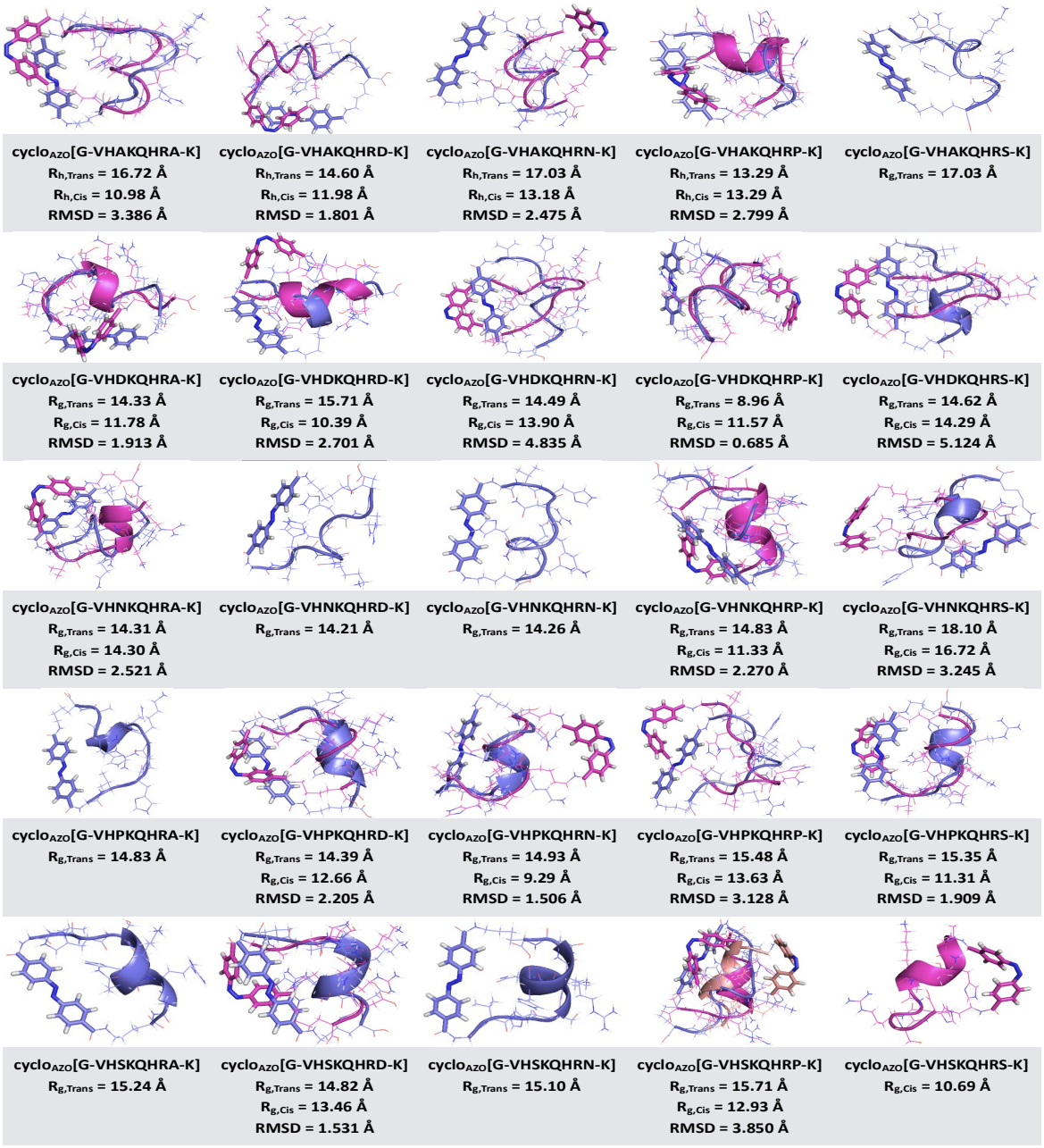

Fig. 2 Structure of 25 variants of the VHPKQHR precursor in the azobenzene-cyclized form cyclo$_{AZOB}$[G-VH(**X**)KQHR(**Z**)-K]-GSG as both cis and trans isomers, and corresponding values of their hydrodynamic radius (R_h) and root mean square deviation (RMSD). Note: the GSG spacer is abstracted for clarity.

Sites S1-5, with a S-score > 0.7, were selected as putative binding pockets on VCAM1. The druggability of these sites, assessed with SiteMap's D-score, featured a D-score > 0.8, supporting their ability to interact with peptide ligand.

We then designed a focused library of 25 variants of the VHPKQHR precursor in the azobenzene-cyclized form cyclo$_{AZOB}$[G-VH(X)KQHR(Z)-K]-GSG (Fig. 1) by varying the positions (X) and (Z) with A, D, N, P, or S. These five amino acids were chosen to explore the effect of mild hydrophobicity (A), peptide turn (P), hydrogen bonding (N and S), and incorporation of a negative charge within a positively charged sequence (D). Aromatic amino acids were avoided to ensure water solubility of the selected peptides; sulfur-containing amino acids were also avoided to prevent formation of disulfide bonds and oxidative degradation.

The crystal structures of the linear precursor VHPKQHR and the *cis* and *trans* isomers of the azobenzene-cyclized variants were generated by molecular dynamics (MD), and evaluated to determine the values of *(i)* equivalent hydrodynamic (R_h) radius[78] and *(ii)* root-mean-square deviation of the atomic positions (RMSD) between the *cis* and *trans* isomers. These values are reported in Fig. 2 together with representative structures of the corresponding peptides. The values of R_h, calculated using HydroPro v.10,[79,80] resulted to be 11.7 Å for the linear VHPKQHR precursor, and varied between ~9 Å and

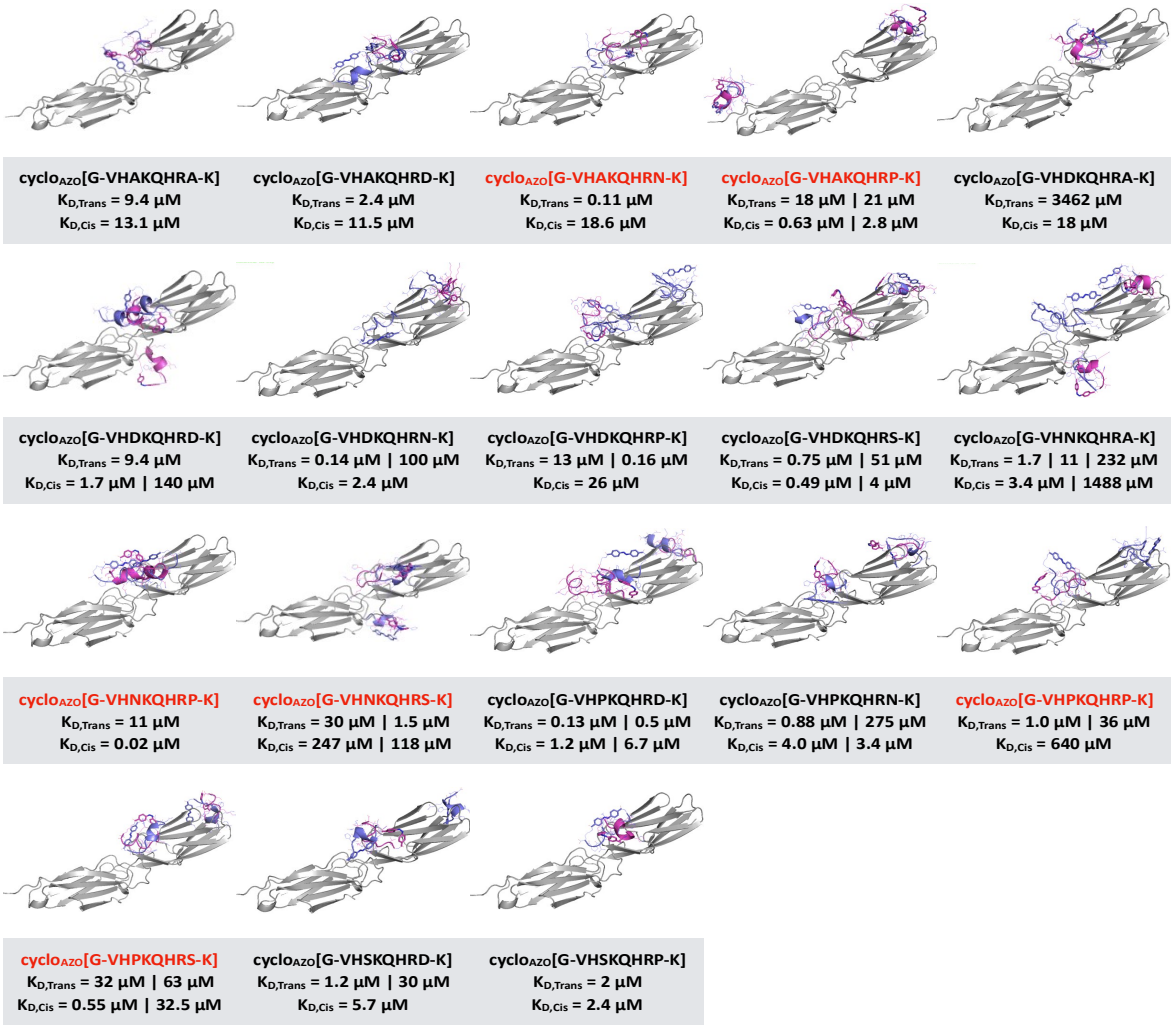

Fig. 3 Structure of the peptide-VCAM1 complexes formed by docking azobenzene-cyclized peptide variants 1-4, 6-11, 14, 15, 17-20, 22, and 24 (Fig. 2) onto the putative binding sites S1-S5 of VCAM1.

~18 Å for the azobenzene-cyclized variants, with an average of 14.9 Å for the *trans* isomers and 12.5 Å for the *cis* isomers. Most notably, the values of atomic *cis*-to-*trans* RMSD fluctuated between ~0.7 Å and ~5.1 Å (average ~3.1 Å), corresponding to a 20 – 25% size shift upon isomerization. Substantial structural rearrangement is critical towards achieving the needed shift in binding affinity. Finally, several variants (*i.e.*, 5, 12, 13, 16, 21, and 23) featured an energy landscape considerably lower – indicating higher stability – in the *trans* configuration, whereas variant 25 showed higher stability in the *cis* configuration. These variants were deemed unable to undergo photo-isomerization and were therefore not considered for the *in silico* screening against VCAM1.

Variants 1-4, 6-11, 14, 15, 17-20, 22, and 24 were docked *in silico* against the putative binding sites S1-S5 on VCAM1 (PDB ID: 1VCA) using HADDOCK (High Ambiguity Driven Protein-Protein Docking, v.2.1)[31,32] following the method employed in prior work.[74,81] In particular, the GSG spacer located on the C-terminus of the peptide was marked as "inactive" to ensure its outward orientation in the peptide-VCAM1 complexes; a short peptide spacer, in fact, is utilized to link the probing moiety (*e.g.*, biotin or a fluorophore) to the peptide and should not be involved in VCAM1 binding. The resulting clusters for every peptide-VCAM1 complex were ranked using the scoring functions FireDock and XScore.[33,34] The top binding complexes were localized mostly on putative binding sites S1, S4, and S5, and were evaluated further by atomistic MD simulations to evaluate the free energy of binding (ΔG_b). Representative examples of modeled peptide-VCAM1 complexes and the corresponding values of binding energy ($\Delta G_{B,Trans}$ and $\Delta G_{B,Cis}$) are shown in Fig. 3.

Variants cyclo$_{AZOB}$[G-VHPKQHRS-K*], cyclo$_{AZOB}$[G-VHAKQHRP-K*], and cyclo$_{AZOB}$[G-VHNKQHRP-K*] were predicted to possess strong binding in *cis* configuration ($\Delta G_{B,Cis}$ < - 8.5 kcal/mol, corresponding to K_D < 0.65 µM), while cyclo$_{AZOB}$[G-VHAKQHRN-K*], cyclo$_{AZOB}$[G-VHNKQHRS-K*], and cyclo$_{AZOB}$[G-VHPKQHRP-K*] were predicted to possess strong binding in *trans* configuration ($\Delta G_{B,Trans}$ < - 7.9 kcal/mol, corresponding to K_D < 1.5 µM). Importantly, these variants were predicted to lose binding upon photo-isomerization ($|\Delta\Delta G_B|$ > 2.5 kcal/mol, highlighted in red) and were therefore selected for experimental analysis. All other variants featured insufficient values of either ΔG_B or $|\Delta\Delta G_B|$ and were therefore abandoned.

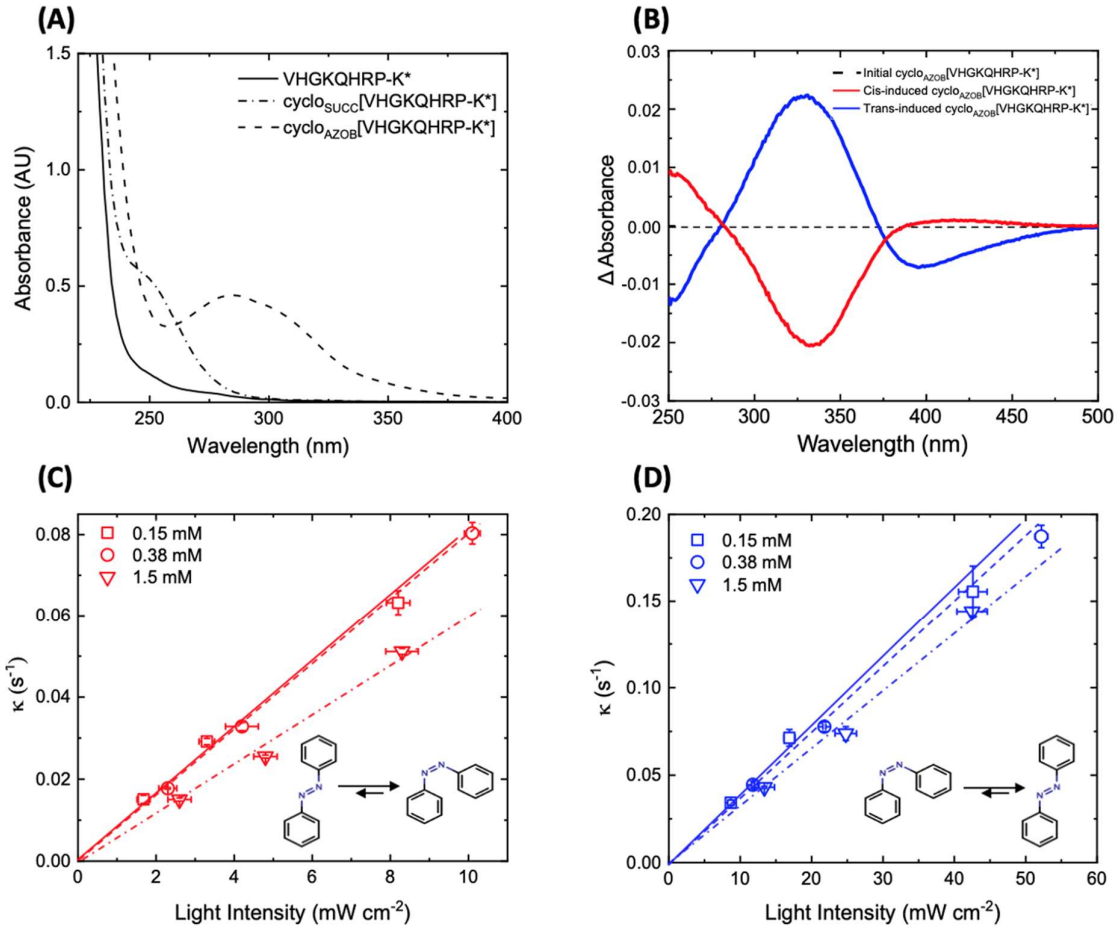

Fig. 4 (A) UV-vis absorption spectra for VHGKQHRP-K* (solid), cyclo$_{SUCC}$[VHGKQHRP-K*] (dot-dash), and cyclo$_{AZOB}$[VHGKQHRP-K*] (dash); (B) Δabsorbance for the cis-induced isomer (red) and trans-induced isomer (blue); (C) *trans-to-cis* isomerization upon exposure to UV light (305-390 nm) and (d) *cis-to-trans* isomerization upon exposure to visible light (>420 nm). For (C) and (D) fitted lines are solid (squares), hash (circles), dot-hash (triangles), and error bars mean ± S.D.

Characterization of azobenzene-cyclized peptides

Spectroscopic characterization

UV spectroscopy was utilized to evaluate the kinetic of photo-isomerization using sequence cyclo$_{AZOB}$[VHGKQHRP-K*] as model variant. The comparison of the absorption spectra of the linear precursor VHGKQHRP-K*, cyclo$_{SUCC}$[VHGKQHRP-K*] (wherein a succinyl linker is utilized in lieu of the azobenzene linker), and cyclo$_{AZOB}$[VHGKQHRP-K*] suggests that: *(i)* peptide cyclization constrains the histidine residues (His), which carry aromatic imidazole rings, in a spatial orientation that produces an increase in absorbance at 254 nm (solid *vs*. dot-dash, Fig. 4A); this effect was reported in a published study on the effect of spatial arrangement of histidine molecules upon their spectroscopic behavior;[82] *(ii)* Cyclization via azobenzene linker magnifies this effect (dot-dash *vs*. dash spectra, Fig. 4A, suggesting interplay between the imidazole residues and the benzene rings in the azobenzene linker; this results in a red shift in absorbance of the peptide segment and a blue shift in the azobenzene absorbance, which have been observed in other azobenzene-cyclized peptides.[83] The histidine-azobenzene interference also attenuates the difference between the spectra of the *trans* and *cis* isomers of cyclo$_{AZOB}$[VHGKQHRP-K*] compared to those characteristic of the *trans* and *cis* isomers of free azobenzene. Despite the subtle difference between the spectroscopic profiles (Fig. 4B), peptide photo-isomerization was detected in the 300 – 390 nm and 400 – 420 nm ranges, corresponding to the π-π* and n-π* bands of azobenzene, respectively. We also recorded the temporal evolution of the spectra of cyclo$_{AZOB}$[VHGKQHRP-K*] in solution during exposure to UV light (using a bandpass light filter BP305-390), and observed a decrease at 340 nm and an increase at 420 nm, both indicative of *trans*-to-*cis* isomerization (Fig. S2A and B); upon exposure to blue light (using a longpass light filter LP420), instead, we observed an increase at 340 nm and a decrease at 420 nm, indicative of *trans*-to-*cis* isomerization (Fig. S2C-D). The difference between the spectra (Δabsorbance) is reported in the inset of Fig. 4B.

Based on the variation in absorbance at 350 nm, the kinetic constants of photo-isomerization were calculated for different values of light intensity and solution concentration (Fig. 4C-D; the data set is reported in the Fig. S3). Rate constants *vs.* exposure intensity were fit, assuming first-order kinetics. The calculated *cis-to-trans* and *trans-to-cis* rate constants are within a factor of 2 of each other; further, the broad excitation spectra and the potentially simultaneous excitation of both *cis-to-trans* and *trans-to-cis* limit direct attribution of the fundamental rate constants to the individual photoisomerization

processes. Accordingly, the reported rate constants are the spectrum-weighted rate constants. The exhibited small difference in the reported rate constants can be attributed to light attenuation by the peptide segment, differences in light attenuation respective to conformation, a difference in photoisomerization cross sections, or the relaxation back to trans may be the favored process. In this context, we believe that the difference stems primarily from a general attenuation phenomenon, as observed at high concentrations, where the light absorbance by the peptide segment reduces the fraction of incident energy absorbed by the azobenzene linkers and, consequently, the isomerization rate. For dilute solutions (0.15 and 0.38 mM), the rate constants of both *trans*-to-*cis* and *cis*-to-*trans* isomerization were found to be higher than the constant obtained with a 1.5 mM (Fig. 4C). At the concentration of 1.5 mM, an attenuation of the excitation energy of approximately 40% is observed across the sample in the BP305-390 range. This effect is illustrated by the larger difference in the rate constants of the *trans-to-cis* isomerization (λ_{ex} = 305-390 nm) across the investigated concentration range (Fig. 4C) compared to the difference in the rate constants of the *cis-to-trans* isomerization (λ_{ex} = 420-500 nm). The effect of light intensity on the rate constant for the *trans-to-cis* isomerization ranges from 7.9 (0.15 and 0.38 mM) to 5.9 $s^{-1}\cdot W^{-1}\cdot cm^2$ (1.5 mM); for the *cis-to-trans* isomerization, the difference is significantly smaller (3.6 - 3.3 $s^{-1}\cdot W^{-1}\cdot cm^2$). This can be attributed to the fact that the absorbance of the peptide significantly decreases beyond 400 nm, which encompasses the LP420-filtered spectra used for the *cis*-to-*trans* isomerization. Notably, the isomerization rate constants of $cyclo_{AZOB}$[VHGKQHRP-K*] are considerably lower than those of free azobenzene and >10-fold lower than that of azobenzene self-assembled monolayers.[84,85]

The slower kinetics are attributed to the covalent linkage of the azobenzene within the framework of the cyclic peptide structure and, potentially, to the aromatic interaction with the histidine residues in the VCAM1-binding peptide segment. It is also noted that the broad spectra used for excitation have a negligible impact on the observed kinetics, as the filtered spectra (Fig. S4) used for excitation feature a narrow peak with the majority of the energy; for the BP305-390 filtered excitation the major peak is at 365 nm, and for LP420 the peak is at 437 nm. The isomerization rate constants were used to calculate the dosage required for a nearly complete (5/κ or 99.3%) photoisomerization: 630 $mJ\cdot cm^{-2}$ for *trans*-to-*cis* isomerization of diluted peptide solutions (0.15 mM and 0.38 mM) and 840 $mJ\cdot cm^{-2}$ for the concentrated solution (1.5 mM); for *cis*-to-*trans* isomerization, the dosage was calculated to be 1400 $mJ\cdot cm^{-2}$ for the diluted solutions and 1500 $mJ\cdot cm^{-2}$ for the concentrated solution. Ackowledging this difference in the *trans-cis* rate constant at high concentration (*i.e.* possible deviation from Beer-Lambert Law) is important as a practical consideration for calculating the dosage needed to achieve complete photoisomerization.

We finally evaluated the ability of $cyclo_{AZOB}$[VHGKQHRP-K*] to undergo multiple cycles of photo-isomerization and the conformational stability of the *cis* isomer at 37°C ("thermal relaxation"). Notably, the photo-isomerization of $cyclo_{AZOB}$[VHGKQHRP-K*] is completely reversible and can be cycled repeatedly (Fig. S5). The thermally induced *cis*-to-*trans* isomerization was evaluated by monitoring the absorbance at 350 nm of a 0.15 mM solution of the *cis* isomer of the peptide for 60 hrs at 37°C (Fig. 5). The resulting half-life of ~44 hrs proves that the *trans* isomer of the peptide is thermally stable within the time span required for cell labelling and imaging without significant unbinding of the peptide. The thermal stability of $cyclo_{AZOB}$[VHGKQHRP-K*] is coherent with the results of the MD simulations, which showed that the energy landscape of the *trans* and *cis* isomers feature minima with similar values, respectively 1063 and 1089 $kJ\cdot mol^{-1}$; these, in turn, are comparable to those of the linear precursor VHPKQHR (958 $kJ\cdot mol^{-1}$) and the cyclic variant $cyclo_{SUCC}$[G-VHAKQHRN-K*] (1035 $kJ\cdot mol^{-1}$), later used in cell labeling.

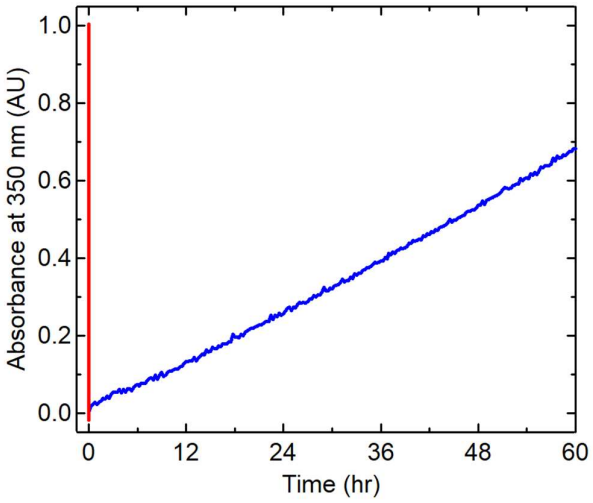

Fig. 5 Thermal *cis-to-trans* isomerization (relaxation) of $cyclo_{AZOB}$[VHGKQHRP-K*]. The red curve represents initial induction of the peptide into the *cis* conformation and the blue curve represents the recovery of the *trans* configuration. Isomerization was monitored by recording the absorbance at 350 nm of a 0.15 mM solution of peptide in MilliQ water for 48 hr, at 37°C in the dark.

These results are particular remarkable considering that, unlike other azobenzene-cyclized variants, neither isomer of $cyclo_{AZOB}$[G-VHAKQHRN-K] features elements of secondary structure (*i.e.*, α-helix or β-sheet) known to confer stability to peptides;[86–88] both VHPKQHR and $cyclo_{SUCC}$[G-VHAKQHRN-K*], in fact, possess a short α-helical segment (Fig. S6C), which contributes to a more favorable energetic state. The secondary structures of $cyclo_{AZOB}$[G-VHAKQHRN-K], VHPKQHR, and $cyclo_{SUCC}$[V-HGKQHRP-K*] predicted *in silico* were confirmed by circular dichroism (Fig. S6).

Lastly, we have conducted a spectroscopic characterization under a broad range of UV light exposure (λ_{ex} = 305-390 nm and λ_{ex} = 420-500 nm) to address concerns of potential cytotoxicity. We note that the dose applied for nearly complete photo-isomerization of the proposed peptide has been reported to cause minimal cytotoxic effects, especially in absence of photosensitizers;[89–93] UV dosing in the range of 138-6000 $mJ\cdot cm^{-2}$ has, in fact, been shown to be viable for multiple cell processing methods.[89–94] The effects of photo-isomerization on cell activity are dependent on several factors, such as the photoisomerization reaction, wavelength, light power, exposure time, and presence of a photosensitizer. It is also noted that the proposed peptide demonstrates thermal stability, indicating that low-dose rapid pulse excitation can be applied to achieve light-induced activation of binding activity. Future efforts should always optimize the operating conditions for each cell-type or target protein, including photoisomerization parameters, to limit cytotoxicity and off-target effects.

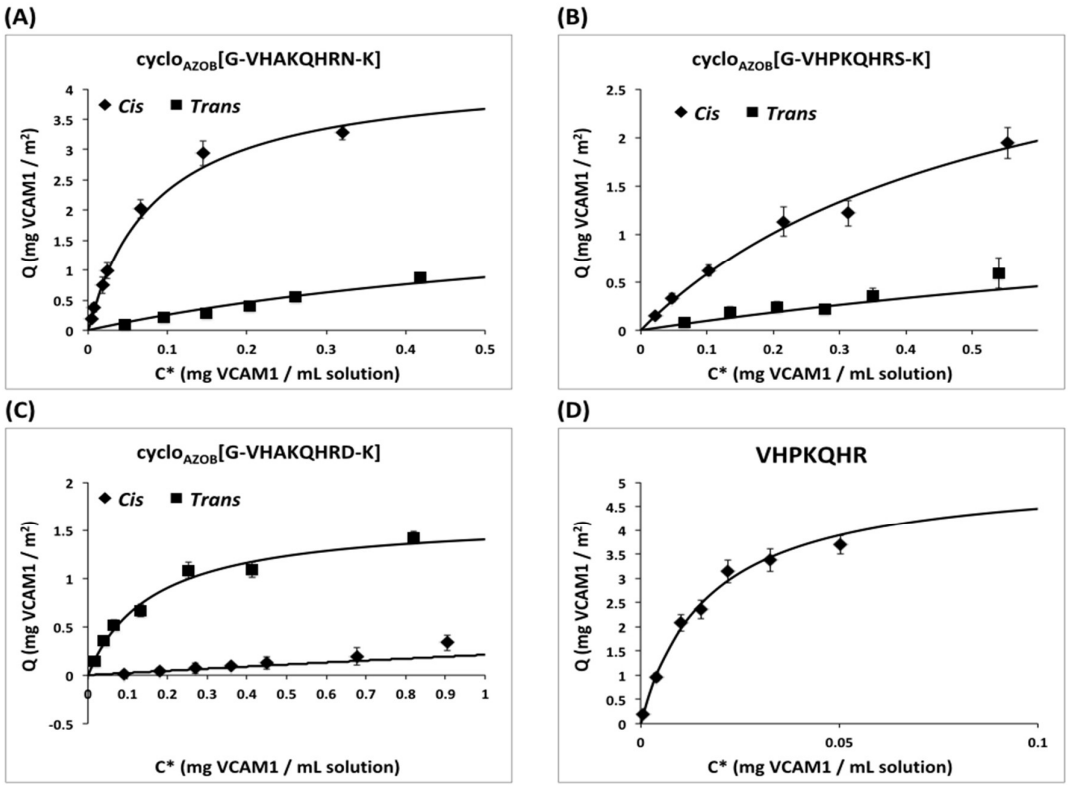

Fig. 6 SPR measurements of VCAM1:peptide $K_{D,Trans}$ and $K_{D,Cis}$ for (A) of cyclo$_{AZOB}$[G-VHAKQHRN-K*]; (B) cyclo$_{AZOB}$[G-VHPKQHRS-K*]; (C) cyclo$_{AZOB}$[G-VHAKQHRD-K*]; and (D) VHPKQHR. The data points were obtained as average of triplicate readings.

Binding affinity by surface plasmon resonance (SPR)

Efficient photo-controlled activation of biorecognition requires a strong shift in binding energy from the inactive to the binding configuration upon photo-isomerization. The *in silico* screening provided several sequences that fulfilled both conditions and were therefore tested by SPR to measure both their $\Delta G_{B,Trans}$ and $\Delta G_{B,Cis}$. The average ligand density for the SPR chips used was 0.86 molecules·nm^{-2}, as reported in Table S2. The values of VCAM1 mass bound to the peptide sensors were fitted to a Langmuir isotherm (Fig. 6), from which the values of K_D were calculated (Table 1). Variant cyclo$_{AZOB}$[G-VHAKQHRN-K*] showed a remarkable variation in binding strength for VCAM1 in solution between the *cis* and *trans* conformations.

Table 1 Values of ΔGB,Trans, ΔGB,Cis, and |ΔΔGB| of the interaction between VCAM1 and cycloAZOB[G-VHAKQHRP-K*], cycloAZOB[G-VHNKQHRP-K*], cycloAZOB[G-VHPKQHRS-K*], cycloAZOB [G-VHAKQHRN-K*], cycloAZOB[G-VHNKQHRS-K*], cycloAZOB[G-VHPKQHRP-K*], and VHPKQHR determined by fitting the VCAM1 adsorption data obtained from the SPR sensorgrams to a Langmuir isotherm. The "---" indicates that no accurate SPR reading could be obtained.

Peptide	$\Delta G_{B,Trans}$ (kcal/mol)	$\Delta G_{B,Cis}$ (kcal/mol)	$\lvert\Delta\Delta G_B\rvert$
cyclo$_{AZOB}$[G-VHAKQHRP-K*]	---	1.09	---
cyclo$_{AZOB}$[G-VHNKQHRP-K*]	1.29	-0.55	1.84
cyclo$_{AZOB}$[G-VHPKQHRS-K*]	3.20	0.68	2.52
cyclo$_{AZOB}$[G-VHAKQHRN-K*]	2.86	-0.07	2.93
cyclo$_{AZOB}$[G-VHNKQHRS-K*]	2.14	---	---
cyclo$_{AZOB}$[G-VHPKQHRP-K*]	1.58	0.06	1.52
VHPKQHR	-0.93		

Cell-labelling with cyclo$_{AZOB}$[G-VHAKQHRN-K*]

The light-activated biorecognition activity of variant cyclo$_{AZOB}$[G-VHAKQHRN-K*] was finally demonstrated *in vitro* via labelling of VCAM1$^+$ BMECs. VCAM1 expression was induced by treating the cells with interleukin-4 (IL-4) and lipopolysaccharide (LPS); this pair has been shown to be synergistic in eliciting VCAM1 expression in endothelial cells.[95–97] VCAM1 expression by BMECs was confirmed by RT-qPCR (Fig. S7); LPS alone also induced VCAM1 expression in BMECs, though to a lesser extent. Human umbilical vein endothelial cells (HUVECs) and human dermal fibroblasts (HDFn) were also considered, but they did not demonstrate significant changes in VCAM1 expression when treated with either condition.

VCAM1$^+$ BMECs were incubated with either the *cis* or *trans* isomer of cyclo$_{AZOB}$[G-VHAKQHRN-K*]-biotin and stained with AlexaFluor488-Streptavidin. As anticipated, the cells labeled with the *cis* isomer demonstrated significantly higher fluorescence intensity compared to those labeled with the *trans* isomer (Fig. 7). The *cis* conformation of cyclo$_{AZOB}$[G-VHAKQHRN-K*] also conferred significantly higher fluorescent intensity to VCAM+ cells compared to VCAM1- cells. To con-

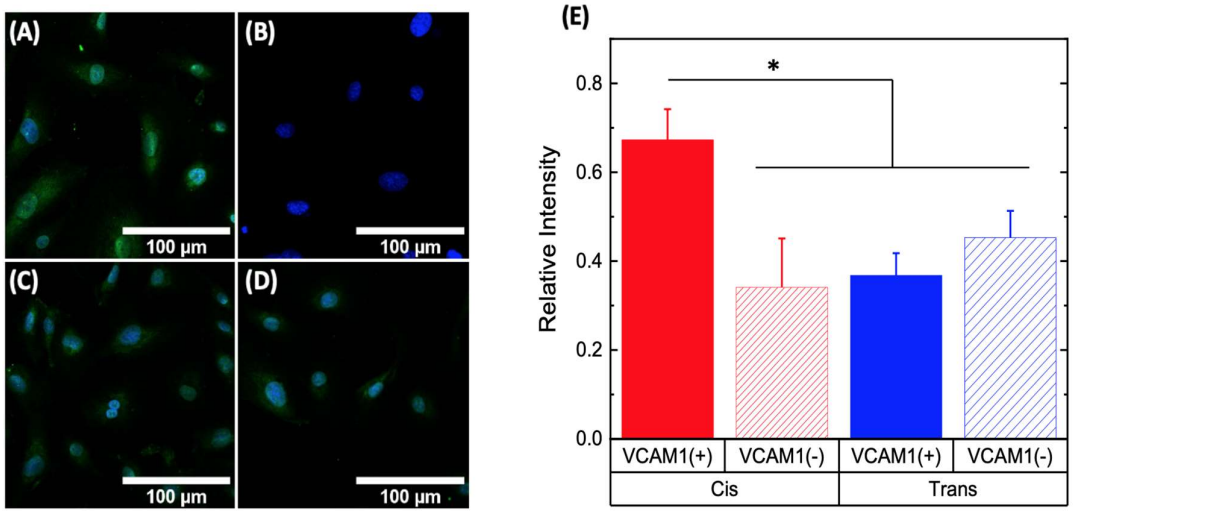

Fig. 7 Cyclo$_{AZOB}$[G-VHAKQHRN-K*] in the *cis* conformation incubated with cells (A) expressing and (B) not expressing VCAM-1, cyclo$_{AZOB}$[G-VHAKQHRN-K*] in the *trans* conformation incubated with cells; (C) expressing and (D) not expressing VCAM-1, and (E) the relative intensity of biotin-labelled cis/trans cyclo$_{AZOB}$[G-VHAKQHRN-K*] incubated with VCAM-1$^{+/-}$ induced cells. Statistics were done with a 2-tailed t-test with a p value < 0.05 (*) considered statistically significant.

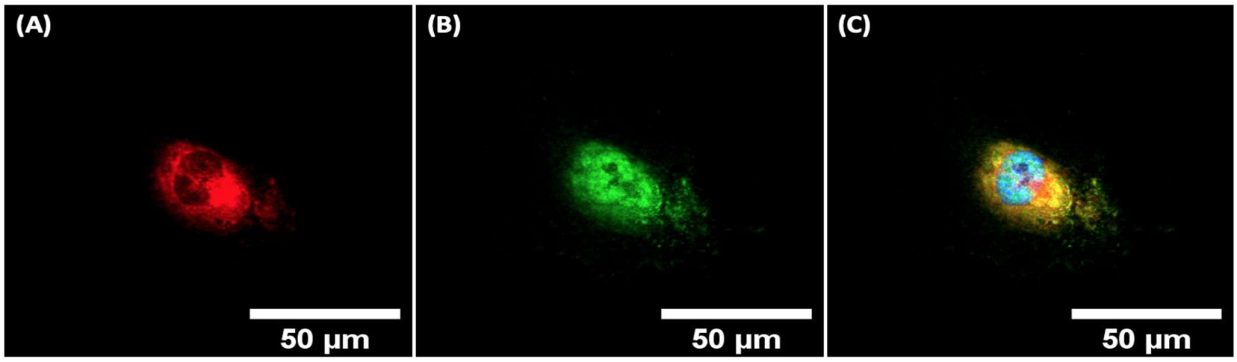

Fig. 8 IL-4/LPS treatment induced VCAM1 expression confirmed with (A) antibody staining (B) *cis* cyclo$_{AZOB}$[G-VHAKQHRN-K*] peptide and (C) the colocalization of the anti-VCAM1 antibody and *cis* cyclo$_{AZOB}$[G-VHAKQHRN-K*] peptide around the nucleus of the cell.

firm selective VCAM1 binding, we also evaluated peptide co-localization with anti-VCAM1 antibodies on VCAM1^{+} BMECs. The images collected using confocal microscopy shows a clear co-localization of the *cis* isomer of cyclo$_{AZOB}$[G-VHAKQHRN-K*] with the VCAM1 antibody (Fig. 8).

Collectively, these results demonstrate both selectivity and light-controlled VCAM1-binding activity of cyclo$_{AZOB}$[G-VHAKQHRN-K*], as well as adequate thermal stability for *in vitro* studies.

Conclusions

The ability to activate – remotely, efficiently, and rapidly – the binding affinity of ligands to target biomolecules will uniquely enable next-generation biotech applications. As more effective mechanisms for affinity regulation are developed, more advanced applications can be explored. To this end, we have developed and demonstrated a novel approach to design and validate azobenzene-cyclized peptide affinity ligands featuring inducible protein-binding activity via light-controlled structural reconfiguration.

Azobenzene-cyclized variants of a known VCAM1-binding peptide (VHPKQHR) were discovered *in silico* that promised isomerization-dependent binding of VCAM1. Selected variants were experimentally characterized for thermal stability, isomerization kinetics, and VCAM1 binding affinity. The selected candidate cyclo$_{AZOB}$[G-VHAKQHRN-K*] was finally tested *in vitro* via light-controlled labelling of VCAM1^{+} BMEC. The peptide showed a statistically significant, conformation-dependent binding selectivity, confirming that the *in silico* and experimental characterizations. This study demonstrates a general method for developing azobenzene-cyclized peptides featuring efficient and robust light-controlled activation of protein-binding affinity. Notably, the light-responsive behavior is imparted to the ligand irrespectively of its protein-binding segment, making our design experimental methods presented herein are applicable to the design of light-responsive labels to virtually any target protein.

These results will enable future studies focusing on the aspects of on-demand, spatio-temporal control, and reversibility of cell labelling. Specifically, future efforts will evaluate *(i)* the kinetics of binding and unbinding the surface of the cells upon exposure to light at activating and de-activating wavelengths; *(ii)* the ability to direct the labelling of a subset of cells in solution via spatial control of the incident light; and *(iii)* the potential downstream effects of the peptide to the cell

surface and, potentially, intracellular metabolic pathways upon binding and unbinding.

Conflicts of interest

There are no conflicts to declare.

Acknowledgements

This work was funded by the National Science Foundation (NSF), award numbers 1743404 and 1653590. This work was also funded, in part, by the American Heart Association Grant 18TPA34230031 and start-up funds provided by NC State University. SM and JDS kindly acknowledge support from the Department of Education Graduate Assistance in Areas of National Need (GAANN) in Molecular Biotechnology. A.T.Y was supported by the Pre-doctoral Training Program in Integrative Vascular Biology at the University of North Carolina at Chapel Hill (NIH 2T32HL069768-16). The authors also wish to thank Dr. E. O. Danilov at the IMAKS lab (Chemistry, NCSU) for his guidance on the UV-Vis measurements.

Notes and references

(1) Valli, H.; Sukhwani, M.; Dovey, S. L.; Peters, K. A.; Donohue, J.; Castro, C. A.; Chu, T.; Marshall, G. R.; Orwig, K. E., *Fertil. Steril.* **2014**, *102* (2), 566-580.e7.
(2) Boxall, S.; Jones, E., *Methods Mol. Biol.* **2015**, *1235*, 121–130.
(3) O'Brien, C. M.; Chy, H. S.; Zhou, Q.; Blumenfeld, S.; Lambshead, J. W.; Liu, X.; Kie, J.; Capaldo, B. D.; Chung, T.-L.; Adams, T. E.; Phan, T.; Bentley, J. D.; McKinstry, W. J.; Oliva, K.; McMurrick, P. J.; et al., *Stem Cells* **2017**, *35* (3), 626–640.
(4) Schröter, C.; Krah, S.; Beck, J.; Könning, D.; Grzeschik, J.; Valldorf, B.; Zielonka, S.; Kolmar, H., *Methods Mol. Biol.* **2018**, *1685*, 311–331.
(5) Plouffe, B. D.; Murthy, S. K., *Anal. Chem.* **2014**, *86* (23), 11481–11488.
(6) Gao, Y.; Li, W.; Pappas, D., *Analyst* **2013**, *138* (17), 4714–4721.
(7) Lam, K. S., Affinity Selection and Sequencing. *Nat. Chem. Biol.* **2019**, *15* (4), 320–321.
(8) Heinis, C.; Winter, G., *Curr. Opin. Chem. Biol.* **2015**, *26*, 89–98.
(9) Shivange, A. V.; Daugherty, P. S., *Methods Mol. Biol.* **2015**, *1248*, 139–153.
(10) Zorzi, A.; Deyle, K.; Heinis, C., *Curr. Opin. Chem. Biol.* **2017**, *38*, 24–29.
(11) Jiang, L.; Wen, L., Photonic Sensitive Switchable Materials. In *Switchable and Responsive Surfaces and Materials for Biomedical Applications*; Zhang, Z., Ed.; Woodhead Publishing: Oxford, 2015; pp 93–118.
(12) Lerch, M. M.; Hansen, M. J.; van Dam, G. M.; Szymanski, W.; Feringa, B. L., *Angew. Chem. Int. Ed.* **2016**, *55* (37), 10978–10999.
(13) Wiedbrauk, S.; Dube, H. *Tetrahedron Lett.* **2015**, *56* (29), 4266–4274.
(14) Wiedbrauk, S.; Bartelmann, T.; Thumser, S.; Mayer, P.; Dube, H., *Nat. Commun.* **2018**, *9* (1), 1–9.
(15) Kitzig, S.; Thilemann, M.; Cordes, T.; Rück-Braun, K., *ChemPhysChem* **2016**, *17* (9), 1252–1263.
(16) Balmond, E. I.; Tautges, B. K.; Faulkner, A. L.; Or, V. W.; Hodur, B. M.; Shaw, J. T.; Louie, A. Y., *J. Org. Chem.* **2016**, *81* (19), 8744–8758.
(17) Cardano, F.; Canto, E. D.; Giordani, S., *Dalton Trans.* **2019**, *48* (41), 15537–15544.
(18) Walkey, M. C.; Peiris, C. R.; Ciampi, S.; C. Aragonès, A.; Domínguez-Espíndola, R. B.; Jago, D.; Pulbrook, T.; Skelton, B. W.; Sobolev, A. N.; Díez Pérez, I.; et al., *ACS Appl. Mater. Interfaces* **2019**, *11* (40), 36886–36894.
(19) Ailuno, G.; Baldassari, S.; Zuccari, G.; Schlich, M.; Caviglioli, G., *J. Drug Delivery Sci. Technol.* **2020**, *55*, 101461.
(20) Ulyanova, T.; Scott, L. M.; Priestley, G. V.; Jiang, Y.; Nakamoto, B.; Koni, P. A.; Papayannopoulou, T., *Blood* **2005**, *106* (1), 86–94.
(21) Kondo, M.; Weissman, I. L.; Akashi, K., *Cell* **1997**, *91* (5), 661–672.
(22) Lai, A. Y.; Kondo, M., *J. Exp. Med.* **2006**, *203* (8), 1867–1873.
(23) Liu, C.; Bhattacharjee, G.; Boisvert, W.; Dilley, R.; Edgington, T., *Am. J. Pathol.* **2003**, *163* (5), 1859–1871.
(24) Kelly, K. A.; Nahrendorf, M.; Yu, A. M.; Reynolds, F.; Weissleder, R., *Mol. Imaging Biol.* **2006**, *8* (4), 201–207.
(25) Kuo, C.-H.; Leon, L.; Chung, E. J.; Huang, R.-T.; Sontag, T. J.; Reardon, C. A.; Getz, G. S.; Tirrell, M.; Fang, Y., *J. Mater. Chem. B* **2014**, *2* (46), 8142–8153.
(26) Nahrendorf, M.; Jaffer, F. A.; Kelly, K. A.; Sosnovik, D. E.; Aikawa, E.; Libby, P.; Weissleder, R., *Circulation* **2006**, *114* (14), 1504–1511.
(27) Burns, V. A.; Bobay, B. G.; Basso, A.; Cavanagh, J.; Melander, C., *Bioorg. Med. Chem. Lett.* **2008**, *18* (2), 565–567.
(28) Bobay, B. G.; Butler, L. R.; Cavanagh, J., *Biochem. Pharmacol.* **2014**, *03* (04).
(29) Hess, B.; Kutzner, C.; van der Spoel, D.; Lindahl, E., *J. Chem. Theory Comput.* **2008**, *4* (3), 435–447.
(30) Klepeis, J. L.; Lindorff-Larsen, K.; Dror, R. O.; Shaw, D. E., *Curr. Opin. Struct. Biol.* **2009**, *19* (2), 120–127.
(31) Dominguez, C.; Boelens, R.; Bonvin, A. M. J. J., *J. Am. Chem. Soc.* **2003**, *125* (7), 1731–1737.
(32) de Vries, S. J.; van Dijk, M.; Bonvin, A. M. J. J., *Nat Protoc.* **2010**, *5* (5), 883–897.
(33) Wang, R.; Lai, L.; Wang, S., *J. Comput. Aided Mol. Des.* **2002**, *16* (1), 11–26.
(34) Wang, R.; Lu, Y.; Wang, S., *J. Med. Chem.* **2003**, *46* (12), 2287–2303.
(35) Amblard, M.; Fehrentz, J.-A.; Martinez, J.; Subra, G., *Mol. Biotechnol.* **2006**, *33* (3), 239–254.
(36) Isidro-Llobet, A.; Álvarez, M.; Albericio, F., *Chem. Rev.* **2009**, *109* (6), 2455–2504.
(37) Chandra, K.; Roy, T. K.; Shalev, D. E.; Loyter, A.; Gilon, C.; Gerber, R. B.; Friedler, A., *Angew. Chem. Int. Ed.* **2014**, *53* (36), 9450–9455.
(38) Kaiser, E.; Colescott, R. L.; Bossinger, C. D.; Cook, P. I., *Anal. Biochem.* **1970**, *34* (2), 595–598.
(39) Islam, N.; Gurgel, P. V.; Rojas, O. J.; Carbonell, R. G., *J. Phys. Chem. C* **2014**, *118* (10), 5361–5373.
(40) Islam, N.; Shen, F.; Gurgel, P. V.; Rojas, O. J.; Carbonell, R. G., *Biosens. Bioelectron.* **2014**, *58*, 380–387.
(41) von Maltzahn, G.; Ren, Y.; Park, J.-H.; Min, D.-H.; Kotamraju, V. R.; Jayakumar, J.; Fogal, V.; Sailor, M. J.; Ruoslahti, E.; Bhatia, S. N., *Bioconjugate Chem.* **2008**, *19* (8), 1570–1578.
(42) Jones, E. Y.; Harlos, K.; Bottomley, M. J.; Robinson, R. C.; Driscoll, P. C.; Edwards, R. M.; Clements, J. M.; Dudgeon, T. J.; Stuart, D. I., *Nature* **1995**, *373* (6514), 539–544.

(43) Sastry, G. M.; Adzhigirey, M.; Day, T.; Annabhimoju, R.; Sherman, W., *Aided Mol. Des.* **2013**, *27* (3), 221–234.
(44) Jacobson, M. P.; Friesner, R. A.; Xiang, Z.; Honig, B., *J. Mol. Biol.* **2002**, *320* (3), 597–608.
(45) Shivakumar, D.; Williams, J.; Wu, Y.; Damm, W.; Shelley, J.; Sherman, W., *J. Chem. Theory Comput.* **2010**, *6* (5), 1509–1519.
(46) Halgren, T.A., *Chem. Biol. Drug Des.* **2007**, *69* (2), 146–148.
(47) Halgren, T. A., *J. Chem. Inf. Model.* **2009**, *49* (2), 377–389.
(48) Berendsen, H. J. C.; van der Spoel, D.; van Drunen, R., *Comput. Phys. Commun.* **1995**, *91* (1), 43–56.
(49) Jorgensen, W. L.; Chandrasekhar, J.; Madura, J. D.; Impey, R. W.; Klein, M. L., *J. Chem. Phys.* **1983**, *79* (2), 926–935.
(50) Jorgensen, W. L.; Tirado-Rives, J., *J. Am. Chem. Soc.* **1988**, *110* (6), 1657–1666.
(51) Nguyen, P. H.; Mu, Y.; Stock, G., *Proteins: Struct., Funct., Bioinf.* **2005**, *60* (3), 485–494.
(52) Nguyen, P. H.; Gorbunov, R. D.; Stock, G., *Biophys. J.* **2006**, *91* (4), 1224–1234.
(53) Nguyen, P. H.; Stock, G., *Chem. Phys.* **2006**, *323* (1), 36–44.
(54) Nosé, S., *Mol. Phys.* **1984**, *52* (2), 255–268.
(55) Hoover, W.G., *Phys. Rev. A Gen. Phys.* **1985**, *31* (3), 1695–1697.
(56) Fu, J.; Yang, H.; Wang, J., *Comput. Biol. Chem.* **2018**, *73*, 200–205.
(57) Parrinello, M.; Rahman, A., *J. Appl. Phys.* **1981**, *52* (12), 7182–7190.
(58) Yu, H.; Lin, Y.-S., *Phys. Chem. Chem. Phys.* **2015**, *17* (6), 4210–4219.
(59) Hess, B.; Bekker, H.; Berendsen, H. J. C.; Fraaije, J. G. E. M., *J. Comput. Chem.* **1997**, *18* (12), 1463–1472.
(60) Cheatham, T. E. I.; Miller, J. L.; Fox, T.; Darden, T. A.; Kollman, P. A., *J. Am. Chem. Soc.* **1995**, *117* (14), 4193–4194.
(61) Quimbar, P.; Malik, U.; Sommerhoff, C. P.; Kaas, Q.; Chan, L. Y.; Huang, Y.-H.; Grundhuber, M.; Dunse, K.; Craik, D. J.; Anderson, M. A.; et al., *J. Biol. Chem.* **2013**, *288* (19), 13885–13896.
(62) Hou, T.; Wang, J.; Li, Y.; Wang, W., *J. Chem. Inf. Model.* **2011**, *51* (1), 69–82.
(63) Genheden, S.; Ryde, U., *Expert Opin. Drug Discov.* **2015**, *10* (5), 449–461.
(64) Ulysse, L.; Cubillos, J.; Chmielewski, J., *J. Am. Chem. Soc.* **1995**, *117* (32), 8466–8467.
(65) Flint, D. G.; Kumita, J. R.; Smart, O. S.; Woolley, G. A., *Chem. Biol.* **2002**, *9* (3), 391–397.
(66) Samanta, S.; Woolley, G. A., *ChemBioChem* **2011**, *12* (11), 1712–1723.
(67) Dong, M.; Babalhavaeji, A.; Samanta, S.; Beharry, A. A.; Woolley, G. A., *Acc. Chem. Res.* **2015**, *48* (10), 2662–2670.
(68) Yasuike, N.; Lu, H.; Xia, P.; Woolley, G. A., Intramolecular Cross-Linking of Proteins with Azobenzene-Based Cross-Linkers. In *Methods in Enzymology*; Deiters, A., Ed.; Optochemical Biology; Academic Press, 2019; Vol. 624, pp 129–149.
(69) Nguyen, P. H.; Staudt, H.; Wachtveitl, J.; Stock, G., *J. Phys. Chem. B* **2011**, *115* (44), 13084–13092.
(70) Reis, J. M.; Xu, X.; McDonald, S.; Woloschuk, R. M.; Jaikaran, A. S. I.; Vizeacoumar, F. S.; Woolley, G. A.; Uppalapati, M., *ACS Synth. Biol.* **2018**, *7* (10), 2355–2364.
(71) Babalhavaeji, A.; Woolley, G. A., *Chem. Commun.* **2018**, *54* (13), 1591–1594.
(72) Bellotto, S.; Chen, S.; Rentero Rebollo, I.; Wegner, H. A.; Heinis, C., *J. Am. Chem. Soc.* **2014**, *136* (16), 5880–5883.
(73) Guerrero, L.; Smart, O. S.; Weston, C. J.; Burns, D. C.; Woolley, G. A.; Allemann, R. K., *Angew. Chem. Int. Ed.* **2005**, *44* (47), 7778–7782.
(74) Woolley, G. A.; Jaikaran, A. S. I.; Berezovski, M.; Calarco, J. P.; Krylov, S. N.; Smart, O. S.; Kumita, J. R., *Biochemistry* **2006**, *45* (19), 6075–6084.
(75) Jafari, M. R.; Deng, L.; Kitov, P. I.; Ng, S.; Matochko, W. L.; Tjhung, K. F.; Zeberoff, A.; Elias, A.; Klassen, J. S.; Derda, R., *ACS Chem. Biol.* **2014**, *9* (2), 443–450.
(76) Bayó-Puxan, N.; Rodríguez-Mias, R.; Goldflam, M.; Kotev, M.; Ciudad, S.; Hipolito, C. J.; Varese, M.; Suga, H.; Campos-Olivas, R.; Barril, X.; et al., *ChemMedChem* **2016**, *11* (8), 928–939.
(77) Shaikh, F.; Siu, S. W. I., *Med. Chem. Res.* **2016**, *25*, 1564–1573.
(78) Peirotti, M. B.; Piaggio, M. V.; Deiber, J. A., *J. Sep. Sci.* **2008**, *31* (3), 548–554.
(79) Armstrong, C. T.; Boyle, A. L.; Bromley, E. H. C.; Mahmoud, Z. N.; Smith, L.; Thomson, A. R.; Woolfson, D. N., *Faraday Discuss.* **2009**, *143*, 305–317; discussion 359-372.
(80) Ortega, A.; Amorós, D.; García de la Torre, J., *Biophys. J.* **2011**, *101* (4), 892–898.
(81) Kish, W. S.; Sachi, H.; Naik, A. D.; Roach, M. K.; Bobay, B. G.; Blackburn, R. K.; Menegatti, S.; Carbonell, R. G., *J. Chromatogr. A* **2017**, *1500*, 105–120.
(82) Pal, N. K.; Kryschi, C., *J. Mol. Catal. A: Chem.* **2015**, *404–405*, 27–35.
(83) Wachtveitl, J.; Spörlein, S.; Satzger, H.; Fonrobert, B.; Renner, C.; Behrendt, R.; Oesterhelt, D.; Moroder, L.; Zinth, W., *Biophys. J.* **2004**, *86* (4), 2350–2362.
(84) Krekiehn, N. R.; Müller, M.; Jung, U.; Ulrich, S.; Herges, R.; Magnussen, O. M., *Langmuir* **2015**, *31* (30), 8362–8370.
(85) Samai, S.; Bradley, D. J.; Choi, T. L. Y.; Yan, Y.; Ginger, D. S., *J. Phys. Chem. C* **2017**, *121* (12), 6997–7004.
(86) Kwok, S. C.; Mant, C. T.; Hodges, R. S., *Protein Sci.* **2002**, *11* (6), 1519–1531.
(87) Rathore, N.; Gellman, S. H.; de Pablo, J. J., *Biophys. J.* **2006**, *91* (9), 3425–3435.
(88) Ji, Y.-Y.; Li, Y.-Q., *Eur. Phys. J. E. Soft Matter* **2010**, *32* (1), 103–107.
(89) Bryant, S. J.; Nuttelman, C. R.; Anseth, K. S., *J. Biomater. Sci. Polym. Ed.* **2000**, *11* (5), 439–457.
(90) Fedorovich, N. E.; Oudshoorn, M. H.; van Geemen, D.; Hennink, W. E.; Alblas, J.; Dhert, W. J. A., *Biomaterials* **2009**, *30* (3), 344–353.
(91) Mironi-Harpaz, I.; Wang, D. Y.; Venkatraman, S.; Seliktar, D., *Acta Biomater.* **2012**, *8* (5), 1838–1848.
(92) Williams, C. G.; Malik, A. N.; Kim, T. K.; Manson, P. N.; Elisseeff, J. H., *Biomaterials* **2005**, *26* (11), 1211–1218.
(93) Wong, D. Y.; Ranganath, T.; Kasko, A. M., *PLoS One* **2015**, *10* (9).
(94) Aubin, H.; Nichol, J. W.; Hutson, C. B.; Bae, H.; Sieminski, A. L.; Cropek, D. M.; Akhyari, P.; Khademhosseini, A., *Biomaterials* **2010**, *31* (27), 6941–6951.
(95) Blease, K.; Seybold, J.; Adcock, I. M.; Hellewell, P. G.; Burke-Gaffney, A., *Am. J. Respir. Cell Mol. Biol.* **1998**, *18* (5), 620–630.
(96) Lee, Y. W.; Kühn, H.; Hennig, B.; Neish, A. S.; Toborek, M., *J. Mol. Cell. Cardiol.* **2001**, *33* (1), 83–94.
(97) Wong, D.; Dorovini-Zis, K., *Microvasc. Res.* **1995**, *49* (3), 325–339.